Demonstration of post-growth wavelength control of VCSELs using high-contrast gratings

E. Haglund, J.S. Gustavsson, J. Bengtsson, Ã…. Haglund, A. Larsson, D. Fattal, W. Sorin, M. Tan

HP Laboratories
HPL-2015-70

Keyword(s):

High Contrast Grating; VCSELs; CWDM; Optical interconnects

Abstract:

We demonstrate post-growth wavelength setting of vertical-cavity surface-emitting lasers (VCSELs) using high-contrast gratings (HCGs). By fabricating HCGs with different duty-cycle and period, the HCG reflection phase can be varied, in effect giving different optical cavity lengths for HCG-VCSELs with different grating parameters. This enables fabrication of monolithic multi-wavelength HCG-VCSEL arrays for wavelength-division multiplexing (WDM). The GaAs HCG is suspended in air by selective removal of an InGaP sacrificial layer. Electrically injected 980-nm HCG-VCSELs with sub-mA threshold currents indicate high reflectivity from the GaAs HCGs. Lasing over a wavelength span of 15 nm was achieved, enabling a 4-channel WDM array with 5 nm channel spacing. Device design, fabrication and experimental proof-of-concept are presented.

External Posting Date: August 21, 2015 [Fulltext] Approved for External Publication
Internal Posting Date: August 21, 2015 [Fulltext]

Demonstration of post-growth wavelength control of VCSELs using high-contrast gratings

E. Haglund[1*], J.S. Gustavsson[1], J. Bengtsson[1], Å. Haglund[1], A. Larsson[1], D. Fattal[2], W. Sorin[3], and M. Tan[3]

[1]*Photonics Laboratory, Department of Microtechnology and Nanoscience, Chalmers University of Technology, SE-41296 Göteborg, Sweden*
[2]*LEIA Inc., 2440 Sand Hill Road, Menlo Park, CA 94025, USA*
[3]*HP Labs, 1501 Page Mill Road, Palo Alto, CA 94304-1123, USA*
[*]*erik.haglund@chalmers.se*

Abstract: We demonstrate post-growth wavelength setting of vertical-cavity surface-emitting lasers (VCSELs) using high-contrast gratings (HCGs). By fabricating HCGs with different duty-cycle and period, the HCG reflection phase can be varied, in effect giving different optical cavity lengths for HCG-VCSELs with different grating parameters. This enables fabrication of monolithic multi-wavelength HCG-VCSEL arrays for wavelength-division multiplexing (WDM). The GaAs HCG is suspended in air by selective removal of an InGaP sacrificial layer. Electrically injected 980-nm HCG-VCSELs with sub-mA threshold currents indicate high reflectivity from the GaAs HCGs. Lasing over a wavelength span of 15 nm was achieved, enabling a 4-channel WDM array with 5 nm channel spacing. Device design, fabrication and experimental proof-of-concept are presented.

OCIS codes: : (050.2770) Gratings; (050.6624) Subwavelength structures; (140.7260) Vertical cavity surface emitting lasers.

References and links

1. N. Chitica, J. Carlsson, L.-G. Svensson, and M. Chacinski, "Vertical cavity surface emitting lasers enable high-density ultra-high bandwidth optical interconnects," in Proc. SPIE, (2015).
2. B. G. Lee, D. M. Kuchta, F. E. Doany, P. Schow, C. Pepeljugoski, C. Baks, T. F. Taunay, B. Zhu, M. F. Yan, G. Oulundsen, D. S. Vaidya, W. Luo, and N. Li, "End-to-end multicore multimode fiber optic link operating up to 120 Gb/s," J. Lightwave Technol. **30**(6), 886-892 (2012).
3. J. A. Tatum, D. Gazula, L. A. Graham, J. K. Guenter, R. H. Johnson, J. King, C. Kocot, G. D. Landry, I. Lyubomirsky, D. Vaidya, M. Yan, and F. Tang, "VCSEL-based interconnects for current and future data centers," J. Lightwave Technol. **33**(4), 727-732, (2015).
4. A. Larsson, "Advances in VCSELs for Communication and Sensing," IEEE J. Sel. Top. Quantum Electron. **17**(6), 1552-1567 (2011).
5. D. M. Kuchta, A. V. Rylyakov, F. Doany, C. L. Schow, J. E. Proesel, C. W. Baks, P. Westbergh, J. S. Gustavsson, and A. Larsson, "A 71 Gb/s NRZ modulated 850 nm VCSEL-based optical link," IEEE Photon. Technol. Lett. **27**(6), 577-580 (2015).
6. E. Haglund, P. Westbergh, J. S. Gustavsson, E. P. Haglund, A. Larsson, M. Geen, and A. Joel, "30 GHz bandwidth 850 nm VCSEL with sub-100 fJ/bit energy dissipation at 25–50 Gbit/s," Electron. Lett. **51**(14), 1096-1098 (2015).
7. P. Westbergh, J. S. Gustavsson, and A. Larsson, "VCSEL arrays for multicore fiber interconnects with an aggregate capacity of 240 Gbit/s," IEEE Photon. Technol. Lett. **27**(3), 296-299 (2015).
8. C. J. Chang-Hasnain, M. W. Maeda, J. P. Harbison, L. T. Florez, and C. Lin, "Monolithic multiple wavelength surface emitting laser arrays," J. Lightwave Technol. **9**(12), 1665-1673 (1991).
9. M. Arai, T. Kondo, A. Onomura, A. Matsutani, T. Miyamoto, and F. Koyama, "Multiple-wavelength GaInAs-GaAs vertical cavity surface emitting laser array with extended wavelength span," IEEE J. Sel. Top. Quantum Electron. **9**(5), 1367-1373 (2003).
10. J. Geske, Y. L. Okuno, D. Leonard, and J. Bowers, "Long wavelength two-dimensional WDM vertical cavity surface emitting laser arrays fabricated by nonplanar wafer bonding," IEEE Photon. Technol. Lett. **15**(2), 179-181 (2003).

11. A. Fiore, Y. Akulova, J. Ko, E. Hegblom, and L. Coldren, "Postgrowth tuning of semiconductor vertical cavities for multiple-wavelength laser arrays," IEEE J. Quantum Electron. **35**(4), 616-623 (1999).
12. T. Wipiejewski, M. Peters, E. Hegblom, and L. Coldren, "Vertical-cavity surface-emitting laser diodes with post-growth wavelength adjustment," IEEE Photon. Technol. Lett. **7**(7), 727-729 (1995).
13. P. B. Dayal, T. Sakaguchi, A. Matsutani, and F. Koyama, "Multiple-Wavelength Vertical-Cavity Surface-Emitting Lasers by Grading a Spacer Layer for Short-Reach Wavelength Division Multiplexing Applications," Appl. Phys. Express **2,** 092501 (2009).
14. J. H. E. Kim, L. Chrostowski, E. Bisaillon and D. V. Plant, "DBR, Sub-wavelength grating, and Photonic crystal slab Fabry-Perot cavity design using phase analysis by FDTD," Opt. Express **15**(16), 10330-10339 (2007).
15. V. Karagodsky, B. Pesala, C. Chase, W. Hofmann, F. Koyama, and C. J. Chang-Hasnain, "Monolithically integrated multi-wavelength VCSEL arrays using high-contrast gratings," Opt. Express **18**(2), 694-699 (2010).
16. C. Sciancalepore, B. Bakir, S. Menezo, X. Letartre, D. Bordel, and P. Viktorovitch, "III-V-on-Si Photonic Crystal Vertical-Cavity Surface-Emitting Laser Arrays for Wavelength Division Multiplexing," IEEE Photon. Technol. Lett. **25**(12), 1111-1113 (2013).
17. T. Ansbæk, I.-S. Chung, E. Semenova, and K. Yvind, "1060-nm Tunable Monolithic High Index Contrast Subwavelength Grating VCSEL," IEEE Photon. Technol. Lett. **25**(4), 365-367 (2013).
18. C. Chang-Hasnain, Y. Zhou, M. Huang, and C. Chase, "High-Contrast Grating VCSELs," IEEE J. Sel. Top. Quantum Electron. **15**(3), 869-878 (2009).
19. F. Sugihwo, M. Larson, and J. S. Harris, "Micromachined widely tunable vertical cavity laser diodes," J. Microelectromech. Syst. **7**(1), 48-55 (1998).
20. G. R. Hadley, "Effective index model for vertical-cavity surface-emitting lasers," Opt. Lett. **20**(13), 1483-1485 (1995).
21. M. J. Cich, J. A. Johnson, G. M. Peake, and O. B. Spahn, "Crystallographic dependence of the lateral undercut wet etching rate of InGaP in HCl," Appl. Phys. Lett. **82**(4), 651-653 (2003).
22. S. Inoue, J. Kashino, A. Matsutani, H. Ohtsuki, T. Miyashita and, F. Koyama, "Highly angular dependent high-contrast grating mirror and its application for transverse-mode control if VCSELs," Jpn. J. App. Phys. **53**, 090306 (2014).

1. Introduction

To meet requirements of higher interconnect capacity in datacenters and high performance computing systems, optical interconnects (OIs) are evolving towards higher data rates on several lanes using parallel optical fibers [1]. Even higher aggregate capacities and improved bandwidth densities are enabled by multicore fibers [2]. Yet another technique for increasing capacity and bandwidth density is wavelength division multiplexing (WDM) [3]. The use of multiple wavelengths on multiple fibers with multiple cores, together with higher lane rates enabled by higher speed optoelectronics and electronics, electronic compensation techniques, and multilevel modulation, may eventually provide >100 Tbit/s interconnect cable capacity.

The vertical-cavity surface-emitting laser (VCSEL) is a light source most suitable for OIs [4]. VCSEL-based OIs have reached >70 Gbit/s lane rates [5], low power dissipation at high bit rates [6], and VCSEL arrays together with multicore fibers have enabled 240 Gbit/s aggregate capacity on a single fiber [7]. The use of VCSELs for WDM-OIs would benefit from the development of monolithic multi-wavelength VCSEL arrays. However, monolithic arrays are intrinsically difficult to realize due to the fact that the resonance wavelength of the conventional all-semiconductor VCSEL cavity, defined by the reflection phase of the top and bottom distributed Bragg reflectors (DBRs) and the thickness of the active region separating the DBRs, is set during epitaxial growth. Therefore, modified growth techniques such as nonuniform growth by molecular beam epitaxy [8], growth on nonplanar substrates by metal-organic chemical vapor deposition (MOCVD) [9], as well as assembly techniques such as nonplanar wafer bonding [10] have been investigated to achieve a wavelength variation over the wafer. However, these techniques are not suitable for small-footprint dense VCSEL arrays with arbitrary layout. Various techniques for post-growth intra-cavity phase tuning have also been investigated, including lateral-vertical oxidation [11] and deposition or thinning of an intra-cavity phase tuning layer prior to the deposition of a dielectric top DBR [12, 13].

Another possibility is to replace the top DBR by a subwavelength high-contrast grating (HCG) and make use of the dependence of the HCG reflection phase on the grating parameters. Multi-wavelength emission can then be achieved by varying the HCG period and/or duty cycle

over the VCSEL array in a single lithography and etch step. This technique has been proposed and analyzed theoretically in [14] and [15], and also experimentally demonstrated by optical pumping experiments [16]. However, electrically injected multi-wavelength HCG-VCSEL arrays have not yet been demonstrated. The main reason is that HCGs with exceptionally high reflectivity are needed. In addition, accurate wavelength setting and control require the use of precise nanofabrication techniques as dimensions are sub-wavelength and the HCG reflection phase is strongly dependent on the grating parameters.

Here we report on the first experimental demonstration of post-growth wavelength control of electrically injected VCSELs using HCGs. The HCG-VCSELs are GaAs-based and employ a suspended GaAs HCG as the top mirror. A wavelength span of 15 nm, centered at 985 nm, is covered by varying the HCG duty cycle from 54 to 69%, in good agreement with simulations.

2. WDM HCG-VCSEL design

The phase of the reflection from the suspended HCG is strongly dependent on the grating period, duty cycle, and thickness. Rigorous coupled wave analysis (RCWA) simulations, seen in Fig. 1, show that the GaAs HCG can achieve high reflectivity (>99.8%) for HCGs with a range of different period and duty cycle combinations. The HCGs are designed for transverse magnetic (TM) polarization, meaning that the electric field is perpendicular to the gratings beams. By changing duty cycle and/or period, a reflection phase span of >60° is achievable (Fig. 1b). Therefore, HCG-VCSEL resonators with different HCG parameters will have different phase shifts from the HCG reflection, leading to different resonance wavelengths, as seen in Fig. 2b. To obtain the largest possible wavelength span for the array, the resonance wavelength of the laser cavity must be highly sensitive to the HCG reflection phase. With few exceptions [17], all demonstrated HCG-VCSELs use a top mirror where the HCG reflectivity is boosted by 2-4 DBR pairs [18]. This makes the resonance wavelength relatively insensitive to the HCG reflection phase and a wavelength range of only ~2 nm is obtained by changing the HCG parameters [18]. Even if the DBR pairs are removed, the obtainable wavelength span is still strongly dependent on the configuration of the cavity, in particular the position of the intra-cavity semiconductor-air interface with respect to the standing wave. It is well known from tunable MEMS-VCSEL design that the best tuning efficiency is obtained if the semiconductor-air interface is placed at a node of the standing wave [19]. This cavity configuration is known as an air-coupled cavity. In our air-coupled cavity design (Fig. 3), the air gap below the HCG is $\lambda/2$ thick and the current spreading layer above the active region of $3\lambda/4$ thick. The resonance wavelength and threshold material gain for HCG-VCSELs with different HCG parameters were simulated using a 1-dimensional effective index model [20], with the HCG reflection amplitude and phase from the RCWA simulations. As seen in Fig. 2a and b, a wide wavelength span of 40 nm can be obtained with threshold material gain <500 cm^{-1}, using HCGs with duty cycles of 45-75% and periods around 405 nm.

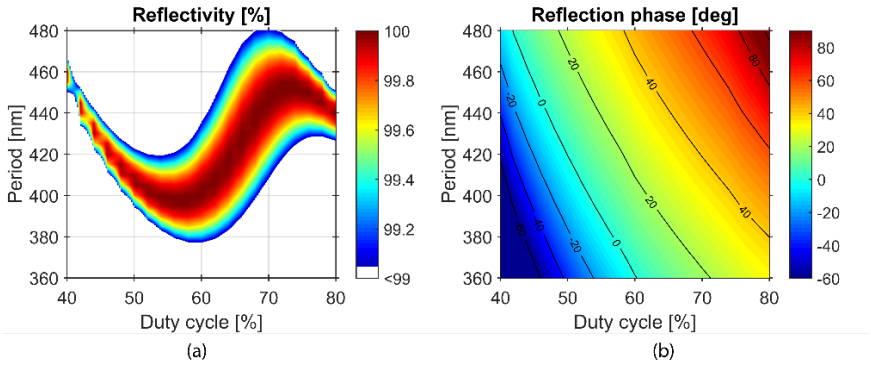

Fig. 1. (a) HCG reflectivity and (b) reflection phase at 980 nm for different grating parameters, simulated by RCWA for a grating thickness of 270 nm.

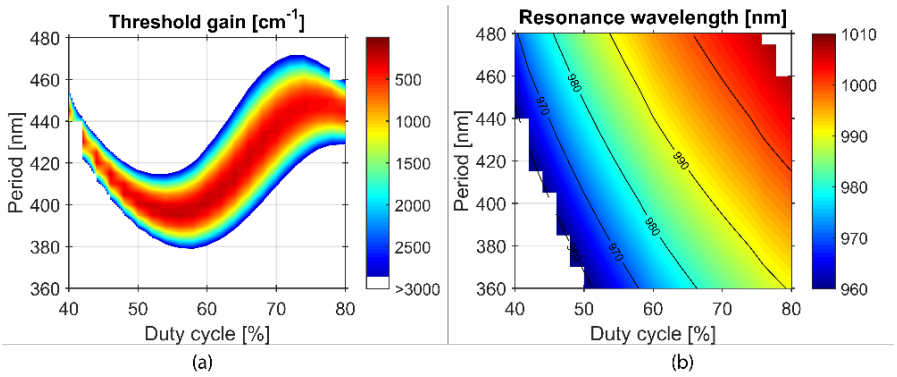

Fig. 2. Simulated (a) material gain at threshold and (b) resonance wavelength for HCG-VCSELs with different HCG parameters.

In the air-coupled cavity configuration the air gap acts as the optical cavity, strongly confining the optical field to the air gap, and the current spreading layer and active region act as the first part of the bottom DBR (see Fig. 3b). The result is a small longitudinal optical confinement factor Γ of around 0.6%. For HCG reflectivties of 99.7%, the numerically calculated material gain at threshold is therefore as high as 1400 cm^{-1}. For an equivalent structure with the semiconductor-air interface at an antinode of the standing wave, the same HCG reflectivity yields a much lower threshold gain of 340 cm^{-1}. However, the achievable wavelength span is then 5-10 times smaller.

A schematic figure of the HCG-VCSEL can be seen in Fig. 3a. The active region features three 6 nm thick strained $In_{0.18}Ga_{0.82}As$ quantum wells with $GaAs_{0.92}P_{0.08}$ strain compensating barriers, with a photoluminescence (PL) wavelength of 970 nm. The bottom *n*-DBR has 37 pairs of $Al_{0.90}Ga_{0.10}As/GaAs$. Holes are injected through the 3λ/4-thick *p*-GaAs current spreading layer which is modulation doped for low resistance and low free-carrier absorption. Transverse current and optical confinement is provided by an oxide aperture on each side of the active region. The 270 nm thick GaAs HCG layer is grown lattice matched on top of the $In_{0.49}Ga_{0.51}P$ sacrificial layer. InGaP was used instead of InAlP [17] or AlGaAs to avoid problems with oxidation of the remaining sacrificial layer. After selective removal, the sacrificial layer forms the λ/2-thick air gap.

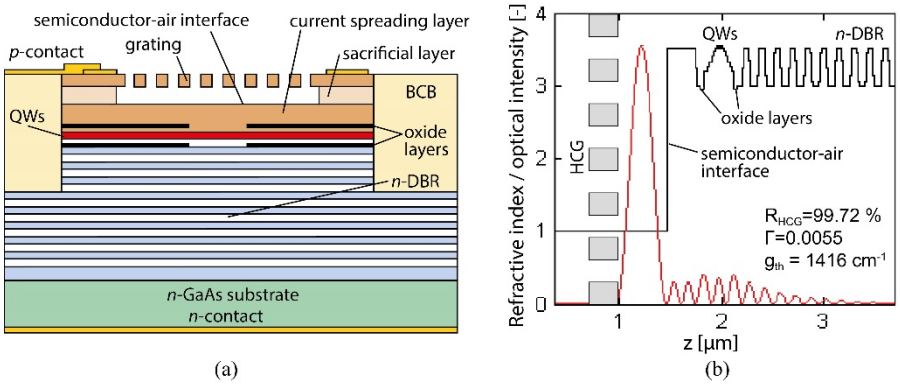

Fig. 3. (a) Schematic figure of the HCG-VCSEL. (b) Refractive index profile and simulated optical field intensity for a HCG-VCSEL with 99.72% HCG reflectivity. The air-coupled design, with an optical field node at the semiconductor-air interface and the optical intensity confined to the air gap, is shown.

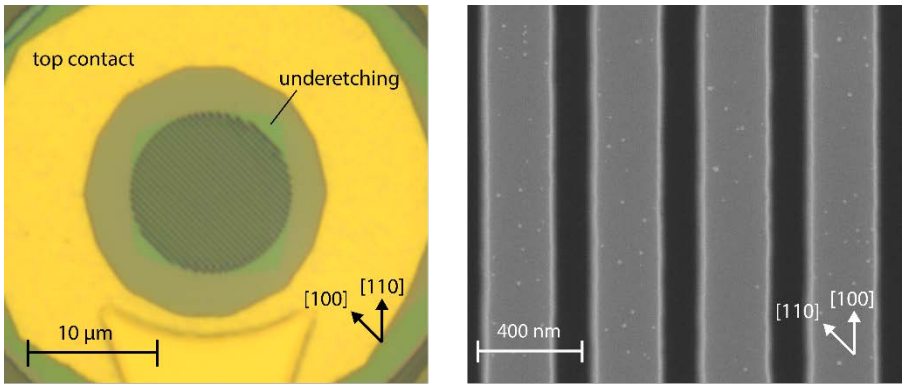

(a) (b)

Fig. 4. (a) Microscope image of a finished HCG-VCSEL. The underetching in the ⟨111⟩ directions is seen in the corners of the HCG. (b) Close-up SEM image of a HCG with a period of 416 nm and duty-cycle of 64%. Note that the images have different crystal orientations.

3. HCG-VCSEL fabrication

The epitaxial structure was grown by MOCVD on an *n*-doped (100) GaAs wafer, with a 10° off-cut towards ⟨111⟩ in order to suppress ordering of the InGaP layer. The multi-wavelength HCG-VCSEL arrays were subsequently fabricated using standard VCSEL processing techniques. First, Ti/Pt/Au top *p*-contacts and Ni/Ge/Au backside *n*-contacts were deposited. Mesas with a diameter of 40-50 µm were then etched in a three-step etch process. Initially, the top GaAs layer was removed using $SiCl_4$/Ar-based inductively coupled plasma (ICP) reactive ion etching (RIE). Since the InGaP of the sacrificial layer etches poorly in this chemistry, it was removed by wet etching using concentrated HCl in a second step. Finally, the ICP-RIE dry etch was used to etch partly into the *n*-DBR to expose the two 30 nm thick $Al_{0.98}Ga_{0.02}As$ layers used for the formation of current apertures in the following selective wet oxidation step. Benzocyclobutene (BCB) was used to planarize the structure and p-bondpads were deposited. The HCGs were defined by electron-beam lithography in 400 nm thick ZEP520A resist. After dry etching into the sacrificial layer using a highly anisotropic $SiCl_4$ RIE dry etch, the sacrificial InGaP layer was selectively removed using concentrated HCl. As the HCl does not etch GaAs, except for the ~1 nm thick native oxide, InGaP may be etched with a selectivity to GaAs approaching infinity. However, the etch rate depends on the crystal orientation and the InGaP will underetch in the ⟨111⟩ directions, but not in the ⟨110⟩ directions [21]. The gratings lines were therefore oriented along ⟨111⟩, at a 45° angle to the {110} cleavage planes. Throughout most of the fabrication, the top surface was protected by a layer of sputtered silicon nitride in order to avoid contamination or unintentional etching. Each resist removal was performed using a combination of standard solvents, O_2-ashing, and ozone cleaning. Especially ozone cleaning was found to be of vital importance for successful removal of the InGaP sacrificial layer. After selective removal, drying was accomplished using critical point drying to avoid stiction. Microscope and close-up SEM images of an HCG-VCSEL with a suspended GaAs HCG are shown in Fig. 4. No buckled grating beams were observed for any fabricated gratings, with diameters up to 22 µm, indicating low stress in the GaAs HCG layer.

4. Measurements

HCG-VCSELs with oxide apertures of 5 µm and different HCG period/duty cycle combinations were characterized by output power and spectral measurements. As seen in Fig. 5a, lasing was observed for a range of different HCG parameters with sub-mA thresholds for several VCSELs. The low threshold currents, despite the air-coupled cavity configuration, indicate very high HCG reflectivity, comparable to, or even better than, that of the top DBRs used in our standard VCSELs. Owing to the angular selectivity of HCGs [22], highly single-mode emission with a

side-mode suppression of 30-40 dB was observed (Fig. 5b). With small variations of the HCG period, and duty cycles from 54 to 69%, lasing over a span of 15 nm was realized, enabling multi-wavelength VCSEL arrays with a channel spacing of 5 nm centered at 985 nm. The observed resonance wavelengths agree well with the 1-D simulations, with a change in the resonance wavelength of 1 nm/duty cycle percentage point, see Fig. 5c.

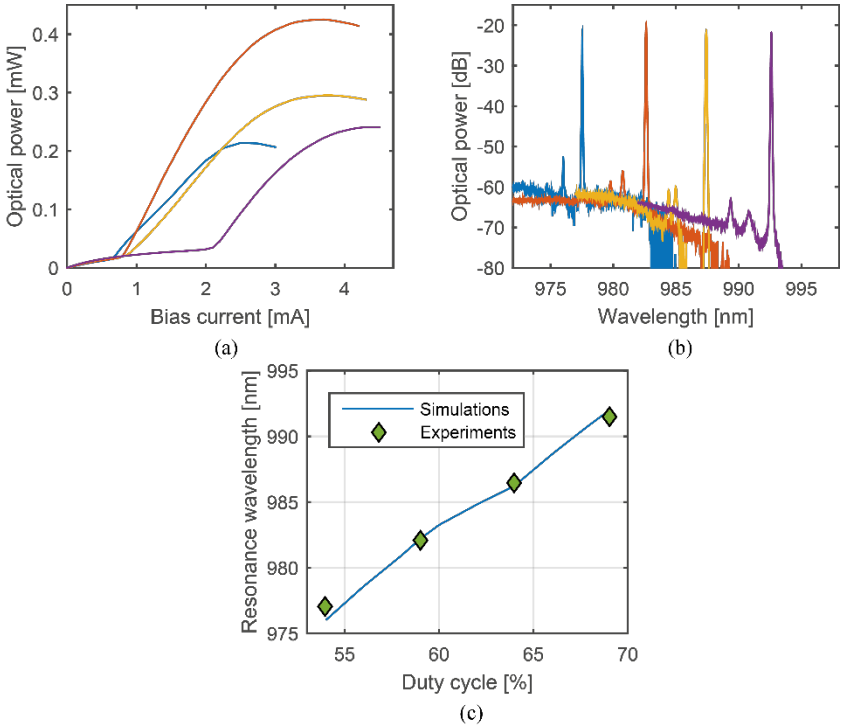

Fig. 5. Characteristics for VCSELs with different HCG period and duty cycle. (a) Output power vs. current. (b) Optical spectra measured at 2 mA (3 mA for the longest-wavelength spectrum). (c) Comparison of measured resonance wavelengths with numerical simulations. The HCG period/duty cycle, from short to long wavelength, is: 405 nm/54%, 405 nm/59%, 400 nm/64%, and 410 nm/69%.

5. Summary and conclusions

The dependence of the HCG reflection phase on the grating parameters was used to demonstrate post-growth wavelength setting of electrically injected HCG-VCSELs. An air-coupled cavity configuration was used to increase the sensitivity of the resonance wavelength to a variation of the grating parameters, thus enabling a large wavelength span. In spite of the low optical confinement factor for this cavity configuration, VCSELs with low threshold currents were demonstrated, indicating very high HCG reflectivities. Lasing was observed over a wavelength span of 15 nm, in excellent agreement with numerical simulations. This has enabled a 4-channel monolithic multi-wavelength VCSEL array with a channel spacing of 5 nm. In addition, this is the first report on suspended GaAs HCGs using an InGaP sacrificial layer, which may be selectively etched with high selectivity.

Acknowledgements

This project was financially supported by Hewlett Packard Labs and the Swedish Foundation for Strategic Research. The authors would also like to acknowledge valuable technical discussions with Dr. Marco Fiorentino and Dr. Sagi Mathai at Hewlett Packard. The epitaxial material was provided by IQE Europe.